Non-rigid Registration of Breast MR Images Using Mutual Information

D. Rueckert[1], C. Hayes[2], C. Studholme[1], P. Summers[1], M. Leach[2], and D. J. Hawkes[1]

[1] Computational Imaging Science Group
Division of Radiological Sciences
UMDS, Guy's Hospital, London SE1 9RT, UK
{email D.Rueckert@umds.ac.uk}
[2] Institute of Cancer Research
CRC Clinical Magnetic Resonance Research Group
Royal Marsden Hospital, Sutton SM2 5PT, UK

Abstract. We present a new approach for the non-rigid registration of contrast-enhanced breast MRI using normalised mutual information. A hierarchical transformation model of the motion of the breast has been developed: The global motion of the breast is modelled using affine transformation models while the local motion of the breast is modelled using spline-based free-form deformation (FFD) models. The algorithm has been applied to the fully automated registration of 3D breast MRI. In particular, we have compared the results of the proposed non-rigid registration algorithm to those obtained using rigid and affine registration techniques. The results clearly indicate that the non-rigid registration algorithm is much better able to recover the motion and deformation of the breast than rigid or affine registration algorithms.

1 Introduction

The application of voxel-based similarity measures for image registration has shown promising results over recent years. In particular, voxel-based similarity measures based on joint entropy [1], mutual information [2–5] and normalised mutual information [6–8] have been shown to align images acquired with different imaging modalities robustly. However, most of the approaches are either limited to rigid or affine transformations or global spline warps with a very limited number of degrees of freedom [9].

The registration of breast MRI is an important task which aids the detection of breast cancer. Currently, the detection and diagnosis of breast cancer primarily relies on X-ray mammography. Even though mammography is highly sensitive, there are a number of disadvantages such as the projective nature of the images and the exposure to radiation. This has led to the investigation of alternative imaging modalities like MRI for the detection of breast cancer. Typically, the detection of breast cancer in MRI requires the injection of a contrast agent whose uptake, it is proposed, will significantly increase the ability to differentiate between different types of malignant and healthy tissue. To quantify the rate of uptake, a 3D MRI scan is acquired prior to the injection of contrast media, followed by a dynamic sequence of 3D MRI scans. The rate of uptake can be

estimated from the difference between pre- and post-contrast images. However, this assessment is complicated by misregistrations caused by patient motion, in particular respiratory motion.

To facilitate the analysis of pre- and post-contrast enhanced MRI, Zuo et al. [10] proposed a registration algorithm which minimises the ratio of variance between images. However, their algorithm is based on the assumption that the breast is only undergoing rigid motion. Kumar et al. [11] proposed a non-rigid registration technique which uses an optical-flow type algorithm and is based on the assumption that the intensities in the pre- and post-contrast enhanced images remain constant. To overcome the problems caused by non-uniform intensity change, Hayton et al. [12] developed a pharmacokinetic model which is used for an optical-flow registration algorithm.

In this paper we will present a new approach for the non-rigid registration of 3D breast MRI. We will use a hierarchical transformation model which captures the global and local motion of the breast. Normalised mutual information is used as a voxel-based similarity measure which is insensitive to changes of intensities between pre- and post-contrast enhanced images and independent of the amount of image overlap.

2 Image Registration

The goal of image registration in contrast-enhanced breast MRI is to relate any point in the post-contrast enhanced sequence to the pre-contrast enhanced reference image, i.e. to find the optimal transformation $\mathbf{T} : (x, y, z) \mapsto (x', y', z')$ which maps any point in the dynamic image sequence $I(x, y, z, t)$ at time t into its corresponding point in the reference image $I(x', y', z', t_0)$ taken at time t_0. In general, the motion of the breast is non-rigid so that rigid or affine transformations alone are not sufficient for the motion correction of breast MRI. Therefore, we develop a combined transformation $\mathbf{T}$ which consists of a global transformation and a local transformation:

$$\mathbf{T}(x, y, z) = \mathbf{T}_{global}(x, y, z) + \mathbf{T}_{local}(x, y, z) \tag{1}$$

2.1 Global motion model

The global motion model describes the overall motion of the breast. The simplest choice is a rigid transformation which is parameterised by six degrees of freedom describing the rotations and translations of the breast. A more general class of transformations are affine transformations which have six additional degrees of freedom describing scaling and shearing. In 3D, an affine transformation can be written as

$$\mathbf{T}_{global}(x, y, z) = \begin{pmatrix} \alpha_{11} & \alpha_{12} & \alpha_{13} \\ \alpha_{21} & \alpha_{22} & \alpha_{23} \\ \alpha_{31} & \alpha_{32} & \alpha_{33} \end{pmatrix} \begin{pmatrix} x \\ y \\ z \end{pmatrix} + \begin{pmatrix} \alpha_{14} \\ \alpha_{24} \\ \alpha_{34} \end{pmatrix} \tag{2}$$

where the coefficients α parameterise the twelve degrees of freedom of the transformation. In a similar fashion the global motion model can be extended to higher-order global transformations such as trilinear or quadratic transformations [13].

2.2 Local motion model

The affine transformation captures only the global motion of the breast. An additional transformation is required which models the local deformation of the breast. The nature of the local deformation of the breast can vary significantly across patients and with age. Therefore, it is difficult to describe the local deformation via parameterised transformations. Instead we have chosen a free-form deformation (FFD) model based on B-splines [14, 15] which is a powerful tool for modelling 3D deformable objects. The basic idea of FFDs is to deform an object by manipulating an underlying mesh of control points. The resulting deformation controls the shape of the 3D object and produces a smooth and C^2 continuous transformation.

To define a spline-based FFD we denote the domain of the image volume as $\Omega = \{(x, y, z) \mid 0 \leq x < X, 0 \leq y < Y, 0 \leq z < Z\}$. Let Φ denote a $n_x \times n_y \times n_z$ mesh of control points $\phi_{i,j,k}$ with uniform spacing. Then, the FFD can be written as the 3D tensor product of the familiar 1D cubic B-splines:

$$\mathbf{T}_{local}(x, y, z) = \sum_{l=0}^{3} \sum_{m=0}^{3} \sum_{n=0}^{3} B_l(u) B_m(v) B_n(w) \phi_{i+l,j+m,k+n} \tag{3}$$

where $i = \lfloor \frac{x}{n_x} \rfloor - 1, j = \lfloor \frac{y}{n_y} \rfloor - 1, k = \lfloor \frac{z}{n_z} \rfloor - 1, u = \frac{x}{n_x} - \lfloor \frac{x}{n_x} \rfloor, v = \frac{y}{n_y} - \lfloor \frac{y}{n_y} \rfloor, w = \frac{z}{n_z} - \lfloor \frac{z}{n_z} \rfloor$ and where B_l represents the l-th basis function of the B-spline [14, 15]

In general, the local deformation of the breast should be characterised by a smooth transformation. To constrain the spline-based FFD transformation to be smooth, one can introduce a penalty term which regularizes the transformation. The general form of such a penalty term has been described by Wahba [16]. In 3D, the penalty term takes the following form:

$$\mathcal{C}_{smooth} = \iiint_{\Omega} \left(\frac{\partial^2 \mathbf{T}}{\partial x^2} \right)^2 + \left(\frac{\partial^2 \mathbf{T}}{\partial y^2} \right)^2 + \left(\frac{\partial^2 \mathbf{T}}{\partial z^2} \right)^2 + 2 \left[\left(\frac{\partial^2 \mathbf{T}}{\partial xy} \right)^2 + \left(\frac{\partial^2 \mathbf{T}}{\partial xz} \right)^2 + \left(\frac{\partial^2 \mathbf{T}}{\partial yz} \right)^2 \right] \tag{4}$$

This quantity is the 3D counterpart of the 2D bending energy of a thin-plate of metal and defines a cost function which is associated with the smoothness of the transformation. Note that the regularization term is zero for any affine transformations and therefore penalises only non-affine transformations.

The degree of local deformation which can be modelled by B-spline FFDs depends essentially on the resolution of the mesh of control points Φ. This enables a hierarchical multi-resolution approach in which the resolution of the control mesh is increased along with the image resolution in a coarse to fine fashion. Finally, B-splines are locally controlled splines which makes them computationally efficient even for a large number of control points compared to thin-plate splines [17] or elastic-body splines [18].

2.3 Normalised Mutual Information

To relate a post-contrast enhanced image to the pre-contrast enhanced reference image, we must define a similarity criterion which measures the degree of alignment between

both images. Given that the image intensity might change after the injection of the contrast agent one cannot use a direct comparison of image intensities, i.e. sum of squared differences or correlation, as a similarity measure. Alternatively one can use mutual information (MI) which has been independently proposed by Collignon [2] and Viola [3, 4] as a voxel-based similarity measure. Mutual information is based on the concept of information theory and expresses the amount of information that one image A contains about a second image B,

$$C_{similarity}(A, B) = H(A) + H(B) - H(A, B) \tag{5}$$

where $H(A), H(B)$ denote the marginal entropies of A, B and $H(A, B)$ denotes their joint entropy which are calculated from the joint histogram of A and B. If both images are aligned the mutual information is maximised. It has been shown by Studholme [6, 7] that mutual information itself is not independent of the overlap between two images. To avoid any dependency on the amount of image overlap, Studholme suggested the use of normalised mutual information (NMI) as a measure of image alignment:

$$C_{similarity}(A, B) = \frac{H(A) + H(B)}{H(A, B)} \tag{6}$$

Similar forms of normalised mutual information have been proposed by Maes et al. [8].

To find the optimal transformation we minimise a cost function as a combination of the cost associated with the smoothness of the transformation C_{smooth} in eq. (4) and the cost associated with the image similarity $C_{similarity}$ in eq. (6):

$$C(\mathbf{T}) = -C_{similarity}(I(t_0), \mathbf{T}(I(t))) + \lambda C_{smooth}(\mathbf{T}) \tag{7}$$

Here λ is the weighting parameter which defines the trade-off between the alignment of the two image volumes and the smoothness of the transformation. We have employed a simple gradient descent technique to minimise the cost function. For computational efficiency, the optimisation proceeds in a multi-resolution fashion: Initially, the affine transformation parameters are optimised at increasing levels of image resolution. During the subsequent refinement the non-affine transformation parameters are optimised at increasing levels of resolution of the control point mesh.

3 Results

We have applied the registration algorithm to volunteer as well as patient data. To test the ability of the algorithm to correct the non-rigid motion of the breast, two separate 3D MR scans of four volunteers were acquired (aged between 28 and 47 years). After the first scan each volunteer was asked to move inside the scanner. For the volunteer studies, a 3D FLASH sequence was used with TR = $12ms$, TE = $5ms$, flip angle = $35°$, FOV = $340mm$ and coronal slice orientation. The MR image were acquired on a 1.5 Tesla Siemens Vision MR system without contrast enhancement. The images have a size of $256 \times 256 \times 64$ voxels and spatial resolution of $1.33mm \times 1.33mm \times 2.5mm$.

Transformation	SSD (mean)	SSD (variance)	CC
-	38.52	53.90	0.8978
Rigid	23.09	33.38	0.9648
Affine	20.67	29.84	0.9736
Affine + FFD ($20mm$)	16.08	23.43	0.9845
Affine + FFD ($15mm$)	14.25	20.91	0.9878
Affine + FFD ($10mm$)	13.07	19.25	0.9899

Table 1. Comparison of the average registration error of the volunteer studies in terms of squared sum of intensity differences (SSD) and correlation coefficient (CC) for different types of transformation. The spline-based FFD has been evaluated at a control point spacing of $20mm$, $15mm$ and $10mm$.

An example of these images is shown in Figure 1. The effect of the misregistration due to the motion of the breast is clearly visible in the difference image. The corresponding registration results based on different transformation models are shown in Figure 2. To assess the quality of the registration in these images in more detail, we have calculated the mean and variance of the squared sum of intensity differences (SSD),

$$SSD = \frac{1}{n}\sqrt{\sum (I(x', y', z', t_0) - I(\mathbf{T}(x, y, z), t_1))^2} \tag{8}$$

as well as the correlation coefficient (CC)

$$CC = \frac{\sum (I(x', y', z', t_0) - \overline{I}(t_0))(I(\mathbf{T}(x, y, z), t_1) - \overline{I}(t_1))}{\sqrt{\sum (I(x', y', z', t_0) - \overline{I}(t_0))^2 \sum (I(\mathbf{T}(x, y, z), t_1) - \overline{I}(t_1))^2}}. \tag{9}$$

Here $\overline{I}(t_0), \overline{I}(t_1)$ denote the average intensities of the images before and after motion and the summation includes all voxels within the overlap of both images. In these images, the squared sum of intensity differences and the correlation coefficient provides a reasonable metric for the assessment of misregistration as the position of the breast tissue changes but the tissue composition and hence image intensity does not. Since the motion of both breasts is normally uncorrelated, we have manually defined a region of interest (ROI) around each breast and then registered both ROIs independently.

Table 1 summarises the results of the registration quality of the volunteer datasets using different transformation models. We have compared three different types of transformations: Pure rigid and affine transformations as well as the proposed non-rigid transformation model which is a combination of an affine transformation and spline-based FFD. The results clearly show that the registrations which are based on rigid or affine transformations improve the correlation between the images before and after motion. However, both transformation models perform significantly worse than the proposed non-rigid transformation model. The results also show that the non-rigid registration performs better as the resolution of the control point mesh of the spline-based FFD increases. While a control point spacing of $20mm$ yields already improved correlation compared to affine transformations, a control point spacing of $15mm$ or less yields even higher correlation. The main reason for this is the increased flexibility of the spline-based FFD to describe local deformations of the breast as the number of control points increases.

Transformation	SSD (mean)	SSD (variance)	CC
–	149.64	205.13	0.8817
Rigid	72.78	91.75	0.9721
Affine	65.12	78.66	0.9784
Affine + FFD ($20mm$)	57.40	68.27	0.9836
Affine + FFD ($15mm$)	54.54	64.69	0.9852
Affine + FFD ($10mm$)	50.13	58.52	0.9877

Table 2. Comparison of the registration error in terms of squared sum of intensity differences (SSD) and correlation coefficient (CC) for the patient study in Figure 3. The region of increased uptake corresponding to the tumour has been excluded.

We have also applied the algorithm to a patient data set with contrast-enhanced MRI. An example of a pre- and post-contrast enhanced image of the patient data set without registration is shown in Figure 3. The difference image shows a substantial amount of motion artefacts. Again, we have used rigid, affine and the proposed non-rigid transformation model for the registration of these images. Figure 4 shows the post-contrast enhanced image and the corresponding difference images after registration. The results demonstrate that all three registrations techniques lead to a significantly improved localisation of the uptake of contrast agent. Again, we have calculated the quality of the registration in terms of squared sum of intensity differences (SSD) and correlation coefficient (CC). The region of increased uptake corresponding to the tumour has been excluded from the calculations. The results are summarised in Table 2 and show that the non-rigid transformation model is better able to correct the motion of the breast than the rigid and affine transformations.

4 Discussion

We have developed a fully automated algorithm for the non-rigid registration of 3D breast MRI based on normalised mutual information. The algorithm uses a non-rigid transformation model to describe the motion of the breast in dynamic MR images. The proposed combination of affine transformations and spline-based FFDs provides a high degree of flexibility to model the motion of the breast. In contrast to physics-based deformation models [19], the algorithm makes no assumptions about the elastic properties of the breast tissue. Even though physics-based deformation models might seem an attractive alternative, for example to model additional constraints such as incompressibility, they are usually difficult to evaluate and verify. Moreover, the elastic properties of the breast tissues can vary significantly across patients and with age which renders the application of such models problematic.

The experimental results have shown that the non-rigid registration of 3D breast MRI can significantly reduce motion artefacts between images. The results have also demonstrated that in many cases rigid or affine registration techniques are not sufficient to correct motion in 3D breast MRI. The registration of these images currently takes between

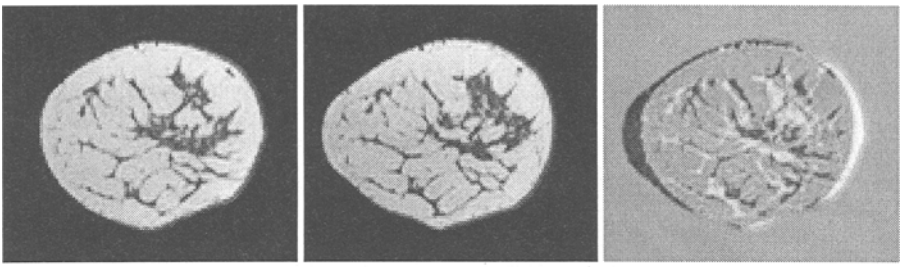

Fig. 1. Example of misregistration caused by motion of a volunteer: (a) before motion, (b) after motion and (c) after subtracting (b) from (a) without registration.

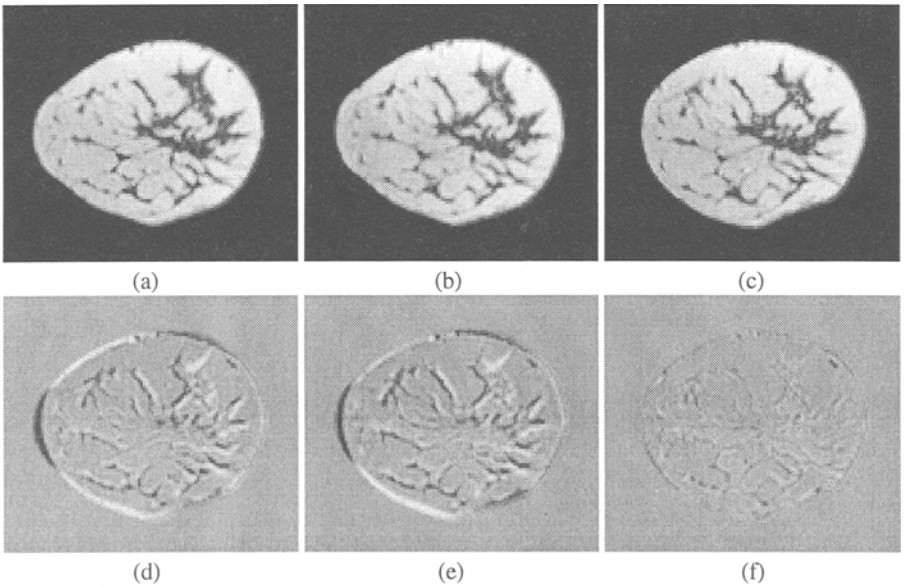

Fig. 2. Example of different transformations on the registration for the volunteer study in Figure 1: After (a) rigid, (b) affine and (c) non-rigid registration. The corresponding difference images are shown in (d) – (f).

15 and 30 *mins.* of CPU time on a Sun Ultra 1 workstation which makes routine application in a clinical environment possible. We have also demonstrated the applicability of the algorithm to the motion correction in contrast-enhanced MRI. However, further work is needed to assess and evaluate the performance of the algorithm in these images. Future work will involve the application of the proposed registration algorithm to data from the MRC-supported UK study of MRI as a method of screening women at genetic risk of breast cancer.

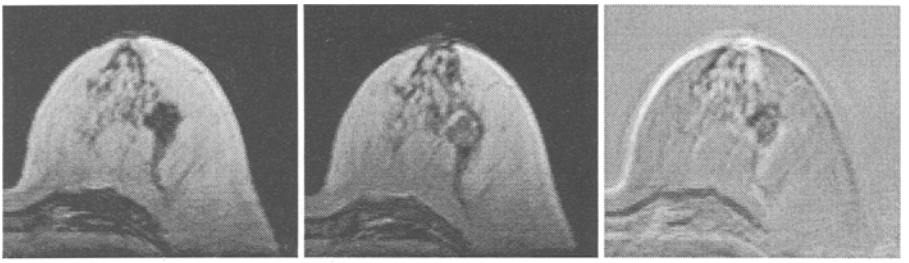

Fig. 3. Example of misregistration in a contrast-enhanced patient study: (a) before injection of the contrast media, (b) after injection of the contrast media and (c) after subtraction of (a) and (b) without registration.

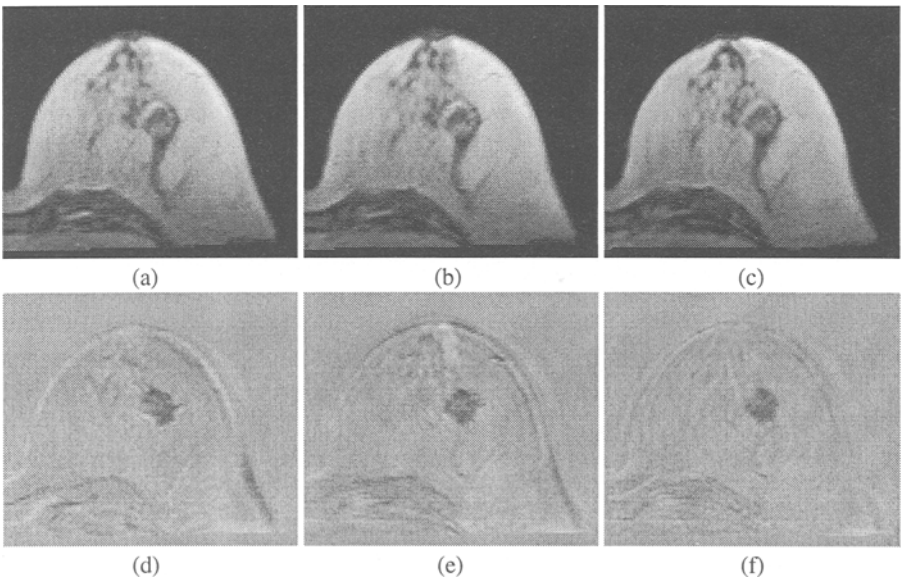

Fig. 4. Example of different transformations on the registration for the patient study in Figure 3: After (a) rigid, (b) affine and (c) non-rigid registration. The corresponding difference images are shown in (d) – (f).

Acknowledgements

We are grateful to EPSRC GR/L08519 for their financial support of this work. The support of the Medical Research Council G9600413 and the Cancer Research Campaign is gratefully acknowledged. We thank Dr. Hubertus Fischer, Siemens (Erlangen) for supplying acquisition sequences for the MRI measurements and the Advisory Group of the MR breast screening study for the measurement protocol.

References

1. C. Studholme, D. L. G. Hill, and D. J. Hawkes. Multiresolution voxel similarity measures for MR-PET registration. In *Information Processing in Medical Imaging: Proc. 14th International Conference (IPMI'95)*, pages 287–298, 1995.
2. A. Collignon, F. Maes, D. Delaere, D. Vandermeulen, P. Seutens, and G. Marchal. Automated multimodality image registration using information theory. In *Information Processing in Medical Imaging: Proc. 14th International Conference (IPMI'95)*, pages 263–274, 1995.
3. P. Viola. *Alignment By Maximization of Mutual Information.* PhD thesis, Massachusetts Institute of Technology. A.I. Technical Report No. 1548., 1995.
4. P. Viola and W. M. Wells. Alignment by maximization of mutual information. *International Journal of Computer Vision*, 24(2):137–154, 1997.
5. C. Studholme, D. L. G. Hill, and D. J. Hawkes. Automated 3-D registration of MR and CT images of the head. *Medical Image Analysis*, 1(2):163–175, 1996.
6. C. Studholme. *Measures of 3D Medical Image Alignment.* PhD thesis, United Medical and Dental Schools of Guy's and St. Thomas's Hospitals, 1997.
7. C. Studholme, D. L. G. Hill, and D. J. Hawkes. An overlap invariant entropy measure of 3D medical image alignment. *Pattern Recognition*, 1998. To appear.
8. F. Maes, A. Collignon, D. Vandermeulen, G. Marechal, and R. Suetens. Multimodality image registration by maximization of mutual information. *IEEE Transactions on Medical Imaging*, 16(2):187–198, 1997.
9. C. R. Meyer, J. L. Boes, B. Kim, P. H. Bland, K. R. Zasadny, P. V. Kison, K. Koral, K. A. Frey, and R. L. Wahl. Demonstration of accuracy and clinical versatility of mutual information for automatic multimodality image fusion using affine and thin-plate spline warped geometric deformations. *Medical Image Analysis*, 1(3):195–207, 1997.
10. C. S. Zuo, A. P. Jiang, B. L. Buff, T. G. Mahon, and T. Z. Wong. Automatic motion correction for breast MR imaging. *Radiology*, 198(3):903–906, 1996.
11. R. Kumar, J. C. Asmuth, K. Hanna, J. Bergen, C. Hulka, D. B. Kopans, R. Weisskoff, and R. Moore. Application of 3D registration for detecting lesions in magnetic resonance breast scans. In *Proc. SPIE Medical Imaging 1996: Image Processing*, volume 2710, pages 646–656, Newport Beach, USA, February 1996. SPIE.
12. P. Hayton, M. Brady, L. Tarassenko, and N. Moore. Analysis of dynamic MR breast images using a model of contrast enhancement. *Medical Image Analysis*, 1(3):207–224, 1997.
13. R. Szelski and S. Lavallee. Matching 3-D anatomical surfaces with non-rigid deformations using octree-splines. In *IEEE Workshop on Biomedical Image Analysis*, pages 144–153, 1994.
14. S. Lee, G. Wolberg, , K.-Y. Chwa, and S. Y. Shin. Image metamorphosis with scattered feature constraints. *IEEE Transactions on Visualization and Computer Graphics*, 2(4):337–354, 1996.
15. S. Lee, G. Wolberg, and S. Y. Shin. Scattered data interpolation with multilevel B-Splines. *IEEE Transactions on Visualization and Computer Graphics*, 3(3):228–244, 1997.
16. G. Wahba. *Spline Models for Observational Data.* Society for Industrial and Applied Mathematics, 1990.
17. F. L. Bookstein. Principal Warps: Thin-plate splines and the decomposition of deformations. *IEEE Transactions on Pattern Analysis and Machine Intelligence*, 11(6):567–585, 1989.
18. M. H. Davis, A. Khotanzad, D. P. Flamig, and S. E. Harms. A physics-based coordinate transformation for 3-D image matching. *IEEE Transactions on Medical Imaging*, 16(3):317–328, 1997.
19. P. J. Edwards, D. L. G. Hill, J. A. Little, and D. J. Hawkes. Deformation for image-guided interventions using a three-component tissue model. In *Information Processing in Medical Imaging: Proc. 15th International Conference (IPMI'97)*, pages 218–231, 1997.